Petroleum Science 23 (2026) 143–156

Contents lists available at ScienceDirect

Petroleum Science

journal homepage: www.keaipublishing.com/en/journals/petroleum-science

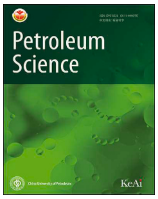

Original Paper

Study on the conductive mechanism and saturation model of continental shale oil reservoirs with complex mineral composition

Yu-Hang Guo [a], Wan-Ying Wang [a,*], Bao-Zhi Pan [a], Shuai Liu [b], Jin-Song Gong [c], Li-Hua Zhang [a], Jia-Yi Zuo [a], Yun-Xiang Gao [a], Xin-Ru Wang [a], Rui-Yi Han [a]

[a] *College of Geo-Exploration Science and Technology, Jilin University, Changchun, 130026, Jilin, China*
[b] *Changji Geological Brigade, Geological Bureau of Xinjiang Uygur Autonomous Region, Changji, 831100, Xinjiang, China*
[c] *Sinopec Jingwei Limited East China Measurement and Control Branch Company, Yangzhou, 225000, Jiangsu, China*

ARTICLE INFO

Article history:
Received 17 February 2025
Received in revised form
23 April 2025
Accepted 13 August 2025
Available online 19 August 2025

Edited by Meng-Jiao Zhou

Keywords:
Shale oil
Pore structure
Digital core
Conductivity simulation
Saturation model

ABSTRACT

A variety of petrophysical experimental techniques were used to analyze the core samples of the Subei Basin, China, and a three-dimensional digital rock model was constructed. The electrical simulation method based on digital rock model was used to clarify the influence of pore structure and complex mineral components (clay minerals, organic matter, metallic minerals) on rock conductivity in the study area. This study, based on petrophysical experiments and digital core technology, proposes a saturation evaluation model that considers the complex mineral composition of the rock and the pore-throat size classification. The newly developed saturation model, constructed using a tri-pore-throat parallel conductive model and fluid distribution model, has demonstrated excellent application potential in the Subei Basin, China. The findings of this study offer a reliable approach for evaluating the saturation of continental shale oil reservoirs.

1. Introduction

In recent years, advancements in oil exploration technology have enabled shale reservoirs to meet the energy demands of many countries. China possesses abundant continental shale oil resources, offering significant exploration potential (Wang et al., 2024). However, compared with conventional reservoirs, shale reservoirs are not only complex in lithology, rich in organic matter, but also have different proportions of inorganic minerals such as quartz, calcite and clay minerals. Moreover, the pore structure and type are complex. There are various types of pores, including not only intergranular pores, but also organic pores, clay pores and other pore types, as well as low porosity and low permeability. Therefore, refining reservoir evaluation techniques is essential for further exploration efforts (Gao et al., 2024).

Resistivity logging is a crucial method for determining reservoir water saturation and plays an irreplaceable role in reservoir evaluation (Lai et al., 2024; Gupta and Kamal, 2023; Zhu et al., 2022; Wang et al., 2022; Wei et al., 2015). Archie (1942) proposed the relationship between resistivity and water saturation in hydrocarbon-bearing formations, establishing a theoretical foundation for using logging data to assess reservoir saturation (Archie, 1942). However, subsequent research revealed that this formula does not apply to reservoirs with high clay content, sparking ongoing exploration for new theories and methods. Many scholars expanded the Archie model by incorporating clay effects, improving its predictive accuracy through clay corrections (Simandoux, 1963; Alger and Raymer, 1963; Poupon et al., 1954; Waxman and Smits, 1968; De Witte, 1955). Schlumberger (1989) introduced the Total Shale model, an enhancement of the Simandoux formula that disregards clay dispersion, which has since been widely applied to saturation calculations in shale reservoirs (Schlumberger, 1989; Sam-Marcus et al., 2018). In addition, some scholars have studied the conduction mechanism of organic matter and further optimized the saturation evaluation model (Kadkhodaie and Rezaee, 2016; Xu et al., 2017). Clavier et al. (1984) introduced the dual-water model, which provided new insights into evaluating hydrocarbon reservoirs with high clay content (Clavier et al., 1984). Subsequently, some scholars have studied the conductive network of the reservoir to improve the prediction

---

* Corresponding author.
E-mail address: wangwy0820@163.com (W.-Y. Wang).
Peer review under the responsibility of China University of Petroleum (Beijing).

https://doi.org/10.1016/j.petsci.2025.08.021
1995-8226/

accuracy of the saturation model (Givens, 1987; Amiri et al., 2015; Mashaba and Altermann, 2015; Hu et al., 2024). With the development of high-precision digital rock technology, the method of combining petrophysical experiment with digital rock technology to evaluate reservoir saturation is gradually emerging (Wu et al., 2020; Zha et al., 2021; Sun et al., 2022).

However, due to the large number of factors affecting shale resistivity and the large differences in shale mineral composition and pore structure in different regions, the applicability of the existing saturation evaluation model is limited. Therefore, it is urgent to propose a shale reservoir saturation evaluation model with wider applicability and comprehensive consideration of pore structure and conductivity mechanism.

This study, based on petrophysical experiments and digital rock technology, develops a saturation evaluation model tailored to the mineral characteristics and pore-throat size. By employing digital rock technology, the conductive mechanism of shale with complex mineral composition is analyzed, ensuring validation between the theoretical model and experimental data. Building on this, a new model combining a tri-pore-throat system with a fluid saturation form is constructed to effectively assess shale oil saturation. This model not only offers theoretical universality but has also proven highly effective in practical applications within the study wells, providing new insights into the evaluation of shale oil saturation.

2. Geological background and experiments

2.1. Regional geological background

The Subei Basin is an onshore part of the South Yellow Sea-Subei continental Mesozoic-Cenozoic basin. The geological profile is shown in Fig. 1. It is in the northern part of Jiangsu Province, China, and extends into the eastern part of Tianchang County, Anhui Province. The basin is bounded by a line running from Jiangdu to Rugao in the south and the coastal area in the north, while to the west it stretches from Sihong to Xuyi and borders the Yellow Sea in the east. It is a Mesozoic Cenozoic fault basin developed on the lower Yangtze Para platform (Fu et al., 2023; Liu et al., 2020).

The study area of this paper is the Gaoyou Sag, which lies in the central part of the Dongtai Depression within the Subei Basin. To the north, the terrain features the Liubao Low Uplift and the Jianhu Uplift, while the western and eastern sections of the sag are marked by the Lintangqiao Low Uplift, the Zheduo Low Uplift and the Wubao Low Uplift, respectively.

The Funing Formation (E_1f) extends across nearly the entire Subei Basin and is well preserved in the basin's sag areas, though it has experienced varying degrees of erosion in the uplift zones. The Funing Formation is subdivided, from bottom to top, into four sections: E_1f_1, E_1f_2, E_1f_3, and E_1f_4. The focus of this study is the E_1f_2, with data derived from well X. The mineral composition in this region is highly variable, and the lithology shows significant changes, which should be carefully considered when designing the subsequent experiments.

2.2. Design of experiments

In this study, we combine the traditional petrophysical experiment method with the numerical simulation method to construct a more universal shale oil saturation evaluation model. X-CT technology was employed to conduct high-resolution scans of typical shale rock samples, enabling the construction of digital core models. These digital cores were then subjected to electrical simulations using the finite element method (FEM) to thoroughly investigate the influence of rock components on electrical conductivity (Liu et al., 2009; Zhao et al., 2013). The workflow is illustrated in Fig. 2.

The experiments followed a systematic process involving rock sample line cutting, sample pretreatment, and rock physics testing. Cylindrical shale samples for porosity evaluation, permeability evaluation and electrical characterization were obtained by wire cutting directional coring. Processed core samples underwent pore-throat size analysis and mineral composition characterization.

Pore structure characterization was achieved through the following petrophysical experiments analyses. (a) The rock resistivity experiments were conducted using the RCS760 Resistivity-Capillary Pressure Measurement System (CoreTest, USA). This system dynamically simulates reservoir temperature, confining pressure, and pore pressure conditions during core flooding to measure

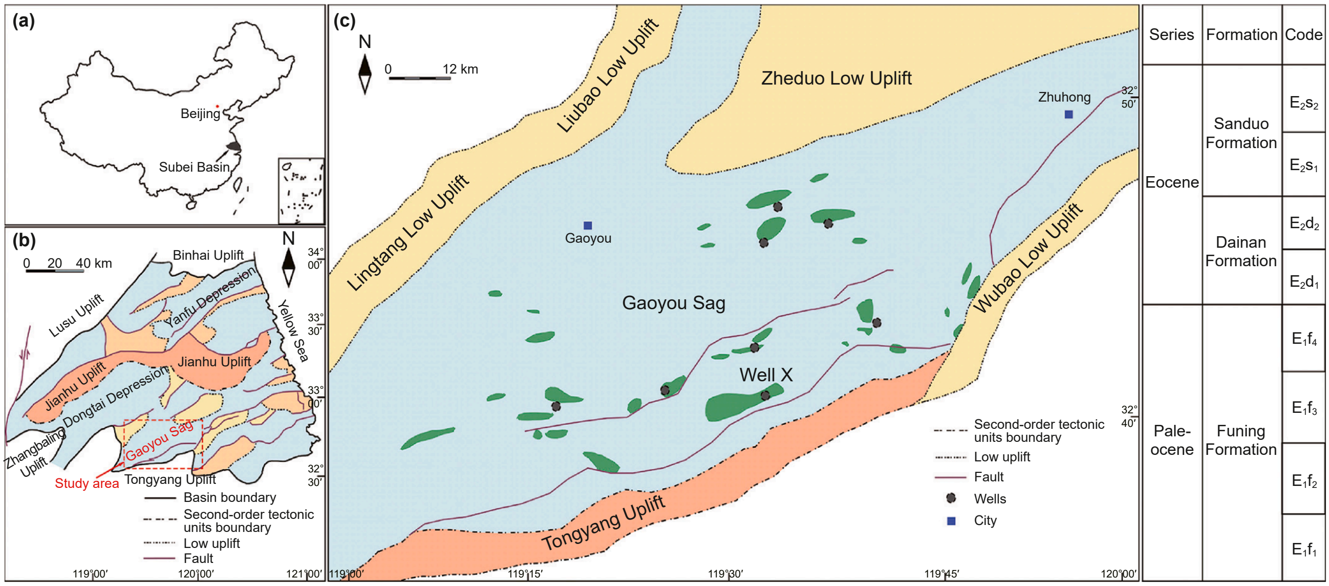

Fig. 1. Characteristics and tectonic evolution of the Subei Basin. **(a)** Schematic map of the area where the North Jiangsu Basin is located; **(b)** geologic overview map of the North Jiangsu Basin; **(c)** geologic overview map of the study area and summary table of the Paleoproterozoic stratigraphy of the North Jiangsu Basin.

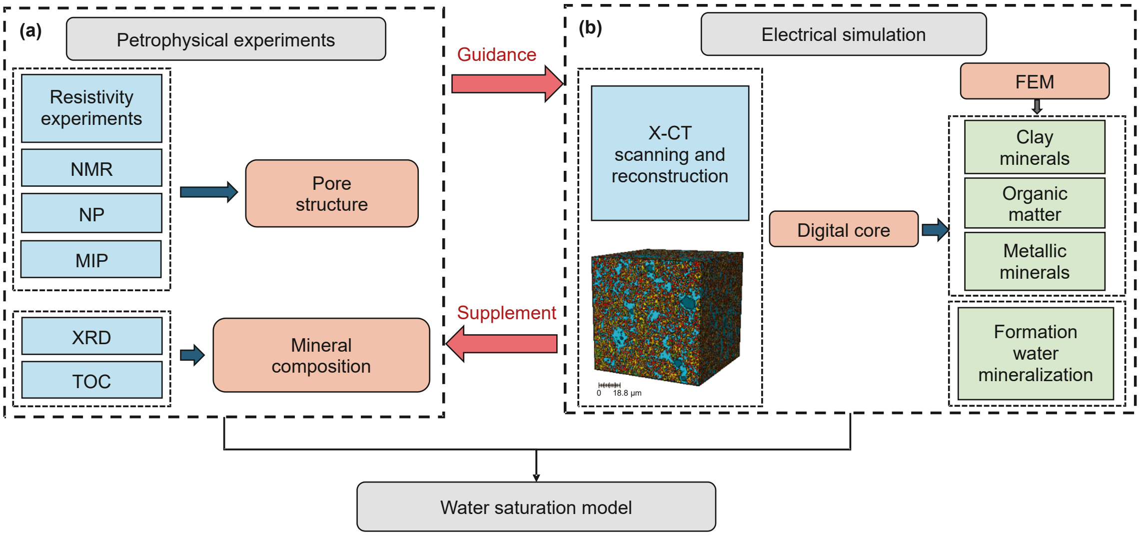

Fig. 2. Numerical simulation combined with petrophysical experiments workflow.

electrical parameters of saturated rock samples. (b) Nuclear magnetic resonance (NMR) experiments were carried out with the MARAN-ULTRA2 Core Analyzer (Oxford Instruments). The method leverages the relaxation behavior of hydrogen nuclei (^{1}H) in pore fluids: transverse relaxation signals (T_2 spectrum) are analyzed to calculate total porosity. Pore-throat size distribution is derived from the linear correlation between relaxation time and pore radius, unaffected by formation water mineralization. (c) Nitrogen physisorption measurements were performed using the AP608 Integrated Porosity-Permeability Analyzer (CoreTest, USA). Based on Boyle's Law, this method quantifies porosity and pore volume by injecting nitrogen gas at controlled pressures into the core and monitoring pressure-volume changes during gas expansion. Total porosity and connected porosity are calculated through mass-volume correlations, providing insights into both open and closed pore networks within the rock matrix. (d) The AutoPore IV 9505 Automated Mercury Porosimeter was employed for mercury intrusion experiments. This technique utilizes non-wetting phase displacement governed by capillary mechanics: mercury is forced into pores under incrementally increased pressure, with smaller pores accessed at higher pressures.

Whole-rock mineral analysis was conducted using a Rigaku SmartLab X-ray diffractometer, a high-resolution instrument for X-ray diffraction (XRD) analysis of rock samples. The experiment is based on the principle that the intensity of diffraction peaks from specific crystalline phases reflects their proportion in the sample. By analyzing diffraction intensity data, we can accurately quantify the crystalline phases in the rock.

Digital core analysis was performed using the Phoenix Nanotom S digital core analysis system. While larger 3D digital cores theoretically capture more details of the rock's microstructure, reflecting its physical properties more accurately, practical limitations such as storage and computational power must be considered. Therefore, an optimal digital core size was chosen to balance simulation accuracy with available computational resources.

3. Experimental results and analysis

3.1. Pore penetration characteristics of samples in the study area

Three types of porosity were measured through petrophysical experiments: porosity (NP), porosity (NMR), and total porosity. The corresponding porosity cross plots are shown in Fig. 3(a). As illustrated, porosity (NP) is significantly lower than total porosity, while porosity (NMR) is slightly lower than total porosity.

This difference arises because porosity (NP) is estimated by measuring the volume or permeability of gas in rock pores. During practical experiments, gases cannot penetrate ineffective pores, such as clay pores, partially disconnected clastic pores, and organic pores. Instead, gases only access the effective pores, leading to an underestimation of gas volume or permeability and thus a lower measured porosity. Effective porosity refers to the connected pores. Total porosity is determined using the weighing method in the laboratory, which is more accurate. During the experiment, a pressure of 30 MPa was applied for pressurized saturation, allowing for the characterization of as many porosity conditions as possible. Porosity (NMR) measures the magnetic nuclei signals within rock pores using NMR technology to infer porosity. The experiment used a frequency of 12 MHz, which is considered an accurate method for characterizing rock porosity. However, shale pores may contain components like non-magnetic organic matter, which NMR struggles to detect, leading to slightly lower porosity readings. Additionally, due to NMR resolution limitations, signals from smaller pores may be lost, further contributing to the slightly lower porosity (NMR) values (Wang et al., 2021; Zhu et al., 2022).

Combining the above analyses, a more accurate total porosity was used for the subsequent study of the shale samples in the study area. To explore the porosity-permeability relationship of the samples in the study area, the cross plot of total porosity and permeability was plotted, as shown in Fig. 3(b), and the porosity-permeability model of the shale in the area was constructed. The permeability K of the rock samples increased with the porosity ϕ increases and is exponentially related to porosity:

$$K = 0.0009 \cdot \exp(238.12\phi) \tag{1}$$

In the formula, the unit of ϕ is %, and the unit of K is mD.

In this study area, there are no obvious fractures in the rock samples, but in fact, the reservoir is a dual-pore system composed of matrix pores and natural fractures, which together determine the permeability of the system. However, since the existing logging methods cannot distinguish the matrix permeability or fracture permeability, most of the previous studies represent the system permeability by calculating the matrix permeability or obtaining the fracture permeability. Subsequently, geophysical logging data can be used to estimate the permeability of the

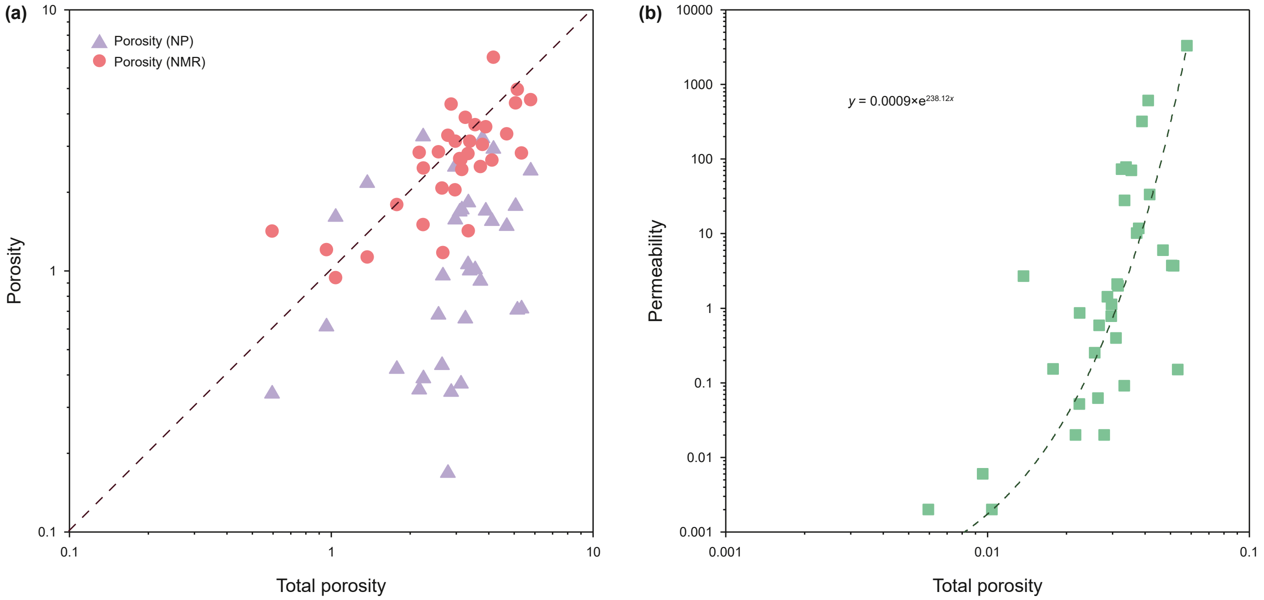

Fig. 3. **(a)** Cross plot of total porosity with porosity measured by other methods; **(b)** cross plot of total porosity with permeability.

system in the study area to improve the correlation between porosity and permeability (Qin et al., 2020).

3.2. Analysis of resistivity experimental results

Archie formula is an empirical relationship between the formation resistivity factor F, porosity ϕ, water saturation S_w and formation resistivity, which is the basis of applying well logging data to quantitatively interpret oil and water formations, and it has simple, practical and clear physical significance. The basic form of Archie formula is given in the following Eqs. (2) and (3):

$$F = R_0/R_w = a/\phi^m \tag{2}$$

$$I = R_t/R_0 = b/S_w^n \tag{3}$$

where a is a lithologic coefficient related to lithology; b is a constant related to lithology; m is the bonding index; n is the saturation index; R_w is the formation water resistivity, Ω·m; R_0 is the 100% saturated formation water rock resistivity, Ω·m; R_t is the formation resistivity, Ω·m; ϕ is the porosity; I is the resistance increasing coefficient.

Through the resistivity experiment, we can get the parameters of the Archie formula. In this study, the rock resistivity analysis data were obtained using the humidified compression drive method, and the results are shown in Fig. 4. From the cross plots, we can see that the application of the traditional Archie formula is not good. As shown in the cross plot of I-S_w in Fig. 4(a), the data points with water saturation (S_w) below 70% are more dispersed, resulting in poor fitting accuracy. This can be attributed to the low porosity and permeability characteristics of shale. Additionally, during the initial stages of the experiment, the humidified immersion method was used, which made it difficult for the brine to fully penetrate the shale's pore spaces. Consequently, the experimental data obtained through the weighing method were poorly fitted and not truly representative. Data points with S_w values above 70% were retained, and the modified cross plot of I-S_w is presented in Fig. 4(b). From Fig. 4(c), it is evident that there are significant variations among the rock samples from the study area. The data distribution is quite scattered, indicating that the lithology of the study area changes greatly, the mineral composition between the different rock samples is more complex and diverse. Therefore, it is necessary to clarify the influence of complex mineral composition on reservoir conductivity to improve the accuracy of saturation evaluation.

3.3. Whole rock mineral content analysis

Whole-rock mineral analysis of the samples from the study area is presented in Fig. 5. The mineral composition shows no significant trend of variation with depth, and there is a wide range in the mineral content, reflecting dramatic lithological changes. Therefore, it is further confirmed experimentally that the study area has complex mineral composition.

The felsic minerals (quartz, orthoclase, and plagioclase) range from 18% to 72%. Carbonate minerals (calcite, dolomite, aragonite, and ankerite) vary between 10% and 75%. Clay minerals (primarily illite, montmorillonite, chlorite and mixed layer, with no kaolinite) account for 6%–40% of the total mineral content. Metallic minerals, mainly pyrite and siderite, are present in minimal quantities, with most samples containing less than 10%. Notably, only one sample, from a depth of approximately 4110 m, shows more than 15% metallic minerals, with occasional high concentrations of siderite in this sample.

These lithological changes greatly influence reservoir space, physical properties, and oil content, resulting in reduced accuracy when using conventional water saturation models. Therefore, it is essential to account for lithological variations when developing a more precise and targeted water saturation model.

3.4. Classification of mineral component

In view of the above researches, we try to divide the rock samples based on mineral composition to improve the accuracy of the saturation evaluation model. The shale in the study area is mainly composed of argillaceous, calcareous and felsic, and the average content of other minerals is less than 5%. According to the core mineral analysis, as shown in Fig. 6(a)–(c), the rock mineral components in the study area are divided into three categories by the method of threshold division. Category 1: Gray argillaceous-

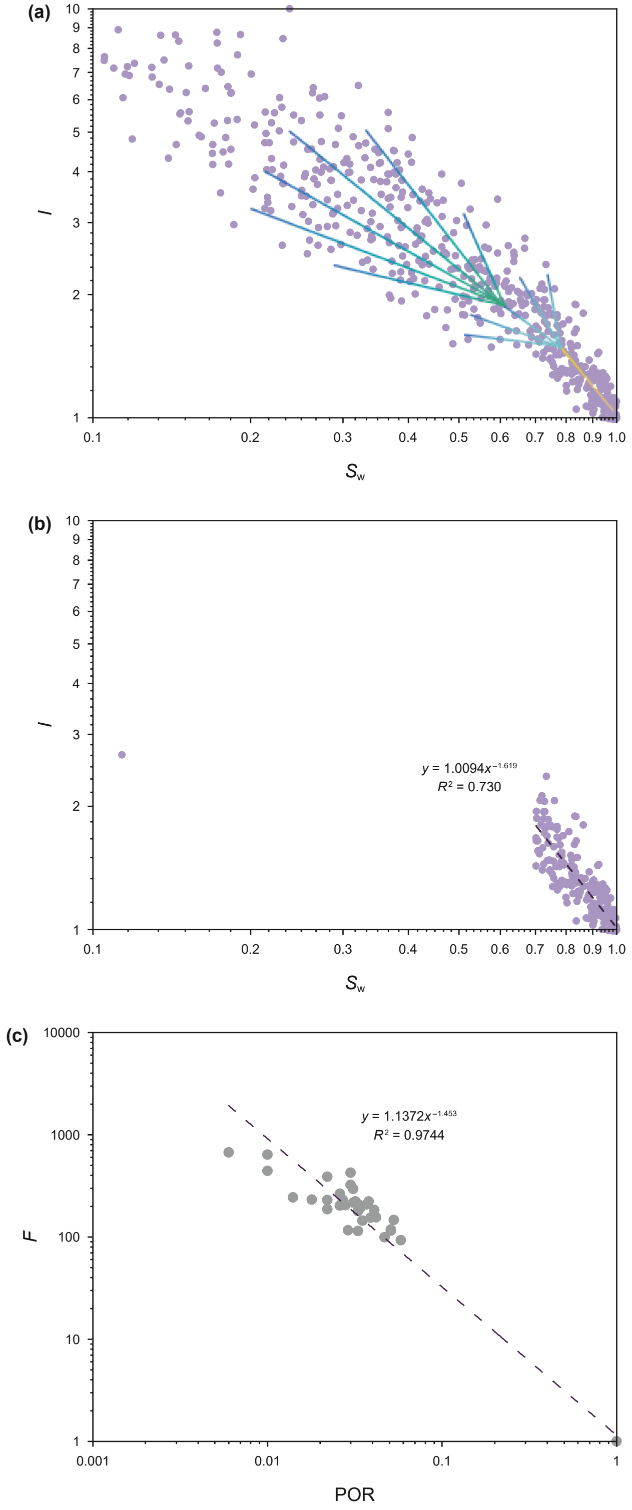

Fig. 4. Cross plots of resistivity experimental results. (**a**) Cross plot of I-S_{w}; (**b**) cross plot of I-S_{w} with S_{w} of 70% or more; (**c**) cross plot of F-POR (POR is the total porosity).

silty hybrid felsic shale is predominantly composed of felsic brittle minerals, with felsic brittle mineral content exceeding 45% and clay mineral content below 30%; Category 2: Gray calcareous-silty hybrid argillaceous shale exhibits elevated clay mineral content, with clay minerals surpassing 35%; Category 3: Felsic-argillaceous hybrid calcareous shale contains carbonate minerals exceeding 45%. The mineral classification triangle is shown in Fig. 6(d).

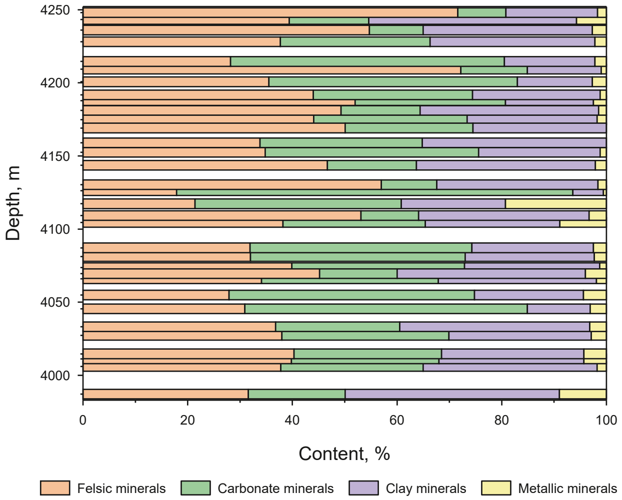

Fig. 5. Plot of mineral content of each component with depth.

3.5. Saturation modeling based on mineral component classification

Since the mineralogical composition of shales in the study area varies widely, and different lithologies affect the pore type, pore distribution and pore throat radius of the rocks, they can indirectly affect the Archie parameters (Moradi and Kadkhodaie, 2024). Therefore, it is first explored whether the classification saturation modeling based on the lithology classification results can effectively improve the accuracy of oil saturation evaluation in this area (see Table 1).

According to Fig. 7, the fitting effect of the cross plots are improved, and there are obvious differences in the Archie parameters between different categories. The saturation index n of Category 1 and Category 2 samples are increased, but the saturation index n of Category 3 sample is still very low, only 1.184. Considering the lithological characteristics of the three types of samples, it is speculated that this is due to the fact that shale has the characteristics of low porosity and low permeability, with low content of free fluids, and most of the conductivity comes from clay water, whereas the clay content of Category 3 sample is low, and the matrix part of the rock has high content, so that this type of samples has a less clay water content, less conductive part, so the n value is lower. However, we need to further verify this hypothesis, so the conductivity mechanism of complex minerals is explained by the method of digital core electrical simulation.

The difference in m between the samples of each category is not significant, indicating that the pore structure and connectivity characteristics of the reservoir are similar. Therefore, based on considering lithology, we further improve the accuracy of the saturation evaluation model by studying the pore throat distribution in the following study (Norbisrath et al., 2015; Tian et al., 2024).

4. Analysis of digital core electrical simulation results

Previous studies have shown that for shale, a self-generating and self-storing unconventional resource, pore structure is the main factor controlling shale oil production. Therefore, the study of pore structure is very important (Chen et al., 2023). In Section 3, we analyzed the pore structure characteristics of shale in the study area through experimental rock physics. In this chapter, we will analyze the pore structure of shale by means of computational

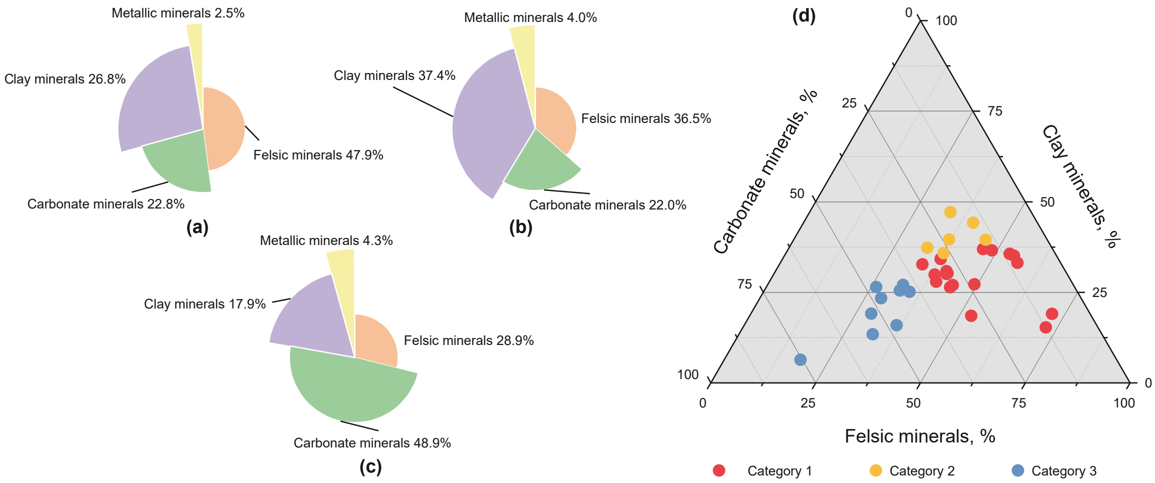

Fig. 6. Classification of lithologic minerals. **(a)** Gray argillaceous-silty hybrid felsic shale (Category 1); **(b)** gray calcareous-silty hybrid argillaceous shale (Category 2); **(c)** felsic-argillaceous hybrid calcareous shale (Category 3); **(d)** mineral classification triangle.

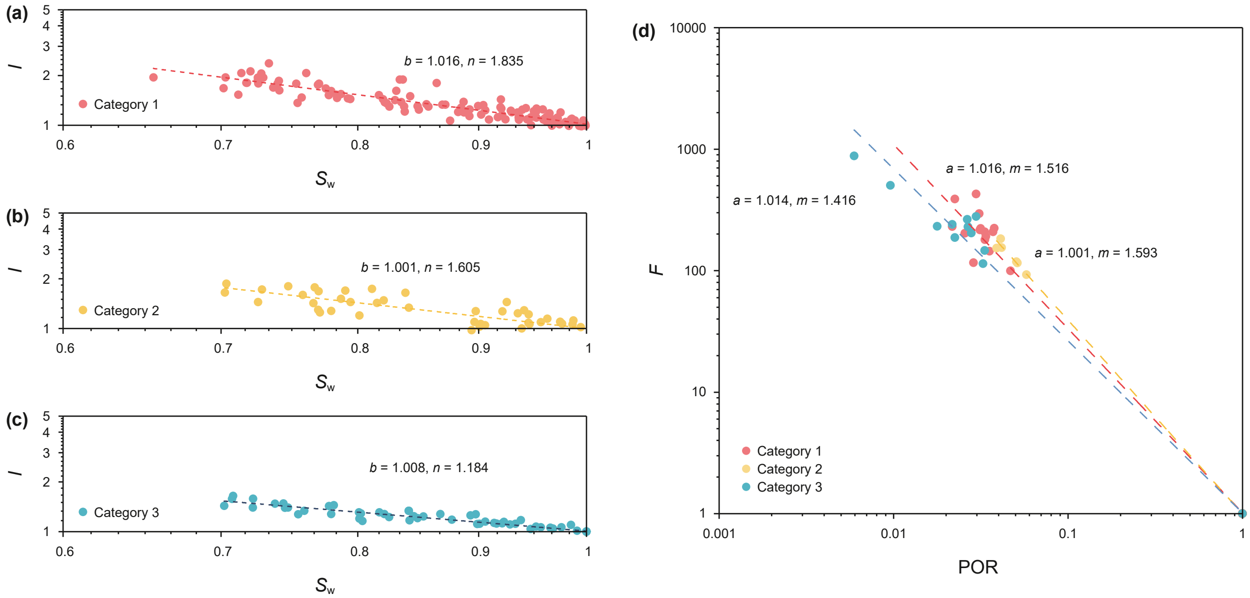

Fig. 7. The cross plots of samples after lithology classification. **(a)** Cross plot of I-S_w for Category 1 samples with 70% or more S_w; **(b)** cross plot of I-S_w for Category 2 samples with 70% or more S_w; **(c)** cross plot of I-S_w for Category 3 samples with 70% or more S_w; **(d)** cross plot of F-POR.

rock physics, that is, digital core method. Combined with its mineralogical characteristics, the numerical simulation of its conductivity is carried out to provide a more solid theoretical basis for our model.

4.1. Construction and simulation of multi-component digital cores

Petrophysical experiments and digital core simulation techniques are employed to thoroughly investigate the properties of reservoir rocks. The research findings provide a reliable basis for understanding how mineral types, pore structures, and other components influence the characteristics of rock samples. Using CT scanning to reconstruct computer images, material information of different densities can be displayed in the form of high-resolution digital images at a specified level (Andhumoudine et al., 2021; Li et al., 2023; Zhou et al., 2024). A 2 mm diameter sample was drilled from a representative area for scanning and three-dimensional model reconstruction, with a resolution of 0.52 μm. Fig. 8 shows a typical two-dimensional grayscale CT scan slice (2 mm in diameter). In this image, the dark black areas represent the pores within the rock sample, while the gray and white areas represent the rock matrix, with the white areas indicating denser material. The brighter the region, the higher the density. Fig. 8(a) illustrates the selection of the matrix area for analysis, with dimensions of 400 × 400 × 400 voxels. During the selection process, fracture areas were avoided, and regions with evenly distributed components were prioritized. On this basis, considering the running performance of the computer, the region with a voxel size of 200 × 200 × 200 is selected. The result is shown in Fig. 8(b). The selected rock samples underwent multi-component threshold segmentation of the matrix section, and the results were compared to the whole-rock analysis, as shown in Table 2. The three-dimensional color display after multi-component threshold segmentation is shown in Fig. 8(c).

4.2. Conductivity analysis

In this study, the finite element method (FEM) was used to simulate the conductive mechanism of shale in the study area.

4.2.1. The effect of mineral composition on rock conductivity

The conductive mechanism of shale is very complex, and the complex mineral composition is one of the main factors. Among the mineral components, the influence of organic matter, clay minerals and metallic minerals on electrical conductivity is particularly obvious. Many scholars have discussed their inherent electrical conductivity, their spatial distribution in the rock, their influence on the overall resistivity of the formation, and the interaction between clay minerals and formation pore water (Liu et al., 2009; Nie et al., 2016; Fan et al., 2020; Li et al., 2022).

By changing the volume fraction and distribution form of metal minerals, the influence of metallic minerals on reservoir conductivity is simulated. The mechanism of the conductivity of organic matter is still unclear, but the research mainly focuses on the discussion of its own conductivity and the conductivity of water in organic pores. Therefore, in this study, the influence of organic matter on reservoir conductivity is simulated by changing the conductivity of organic matter (C_{TOC}) itself and changing the conductivity of formation water (C_{w}) (Wang et al., 2018).

The conductivity of clay minerals is mainly determined by the solid particles and the water in the pores. Therefore, in the process of numerical simulation, we simulate the influence of clay minerals on reservoir conductivity by exploring the different volume fraction and cation exchange capacity of clay minerals (Hasan et al., 2021). Due to ion substitution processes, the surfaces of clay particles develop an excess negative charge. To maintain electrical neutrality, these surfaces adsorb cations from the surrounding formation water. The combination of adsorbed cations and clay particles creates a dipole layer, which strongly affects the conductive properties of the clay mineral assemblages. The cation exchange capacity Q_{v} is a key parameter used to assess the electrical conductivity, which represents the number of exchangeable sodium ions per unit of total pore volume. In the study area, the types of clay minerals contained in the samples are determined, which are illite-montmorillonite mixed layer, illite and chlorite. Table 3 provides the common values of cation exchange capacities for various clay minerals.

Table 1
Table of Archie parameters after sample lithology classification.

Category	*a*	*b*	*m*	*n*
1	1.016	1.016	1.516	1.835
2	1.001	1.001	1.593	1.605
3	1.014	1.008	1.416	1.184

Due to the high irreducible water saturation and low porosity of the reservoir in the study area, the resistivity anisotropy of the reservoir is weak, so only the reservoir resistivity in the *x* direction is discussed (Qin et al., 2023). The different digital core parameters constructed are shown in Table 4.

The results of the electrical simulation are shown in Fig. 9. C_0 represents the electrical conductivity of the whole rock. From Fig. 9(a), it can be observed that as the Q_{v} increase in the clay content, the additional electrical conductivity of the clay enhances with an C_0 increases approximately linearly; the results in Fig. 9(b) show that with the increase of clay content, the C_0 tends to increase, and at clay content less than 40%, the C_0 tends to increase

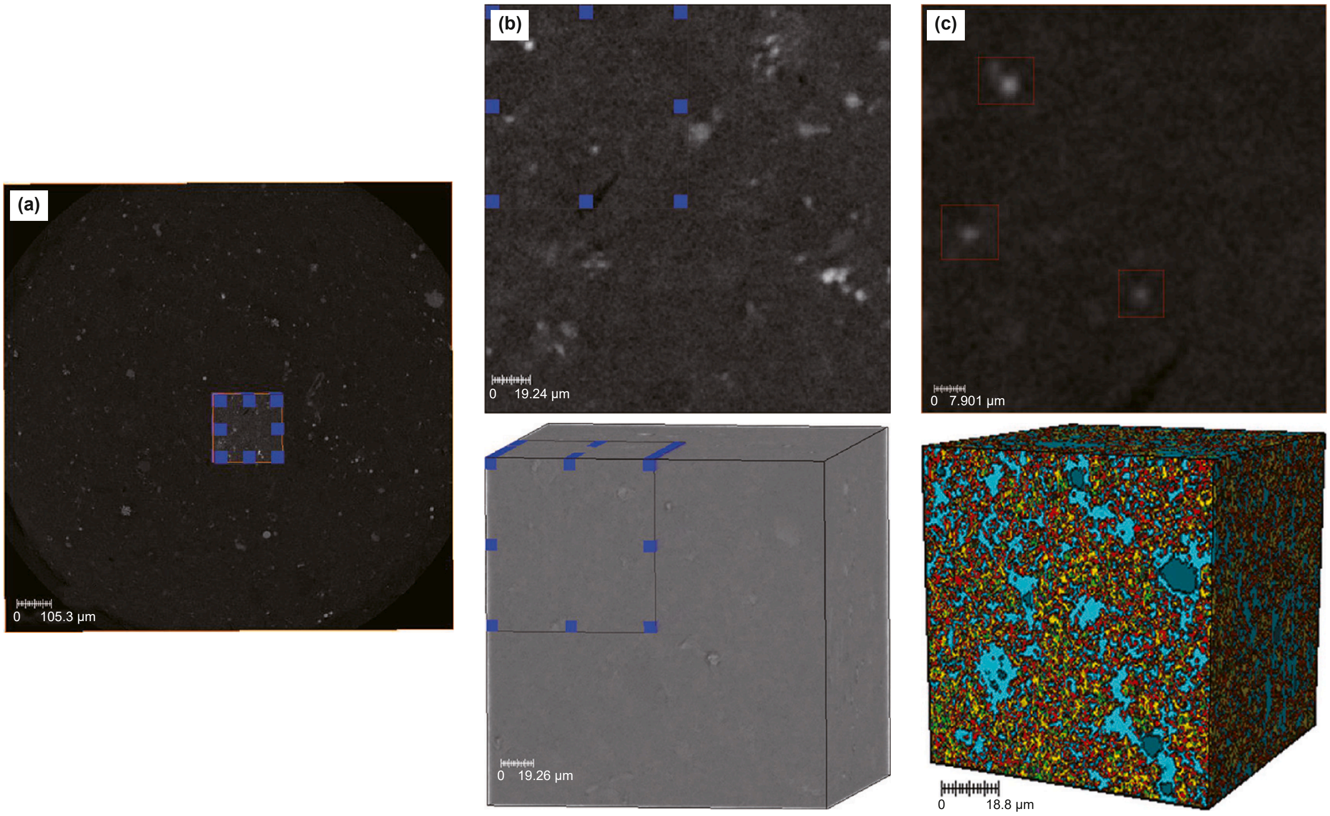

Fig. 8. Establishment of three-dimensional digital core. **(a)** Typical 2D grayscale slices of core samples; **(b)** 2D and 3D display of selected areas with a voxel size of 400 × 400 × 400; **(c)** regionally selected 2D grayscale slices with a voxel size of 200 × 200 × 200 and 3D color display after multicomponent threshold segmentation.

Table 2
Multi-component segmentation results of digital cores.

	POR, %	Felsic minerals, %	Organic matter, %	Carbonate minerals, %	Metallic minerals, %	Clay minerals, %
XRD	2.5865	35.3861	3.6378	29.9749	1.4799	28.2708
400^3	2.5670	36.3220	3.6632	29.9590	1.4596	28.3380
200^3	3.2824	34.4057	4.0006	33.0332	1.5022	26.7296

slowly, and when the clay content increases to more than 40%, the C_0 increases rapidly. Combined with the geological background, we can conclude that the clay content of the rock samples in the study area is mostly less than 40%, and the composition of the clay minerals is basically the same, that is, Q_v has no strong change, so the clay minerals themselves have little effect on the conductivity of the rock. The groundwater conductivity C_w is related to the C_0 relationship is shown in Fig. 9(c), the conductivity of different organic matter showed the same trend, when the formation water conductivity is less than 5 S/m, with the increase of formation water conductivity, it C_0 also increases gradually, and when the formation water conductivity exceeds 5 S/m, the $C_0 - C_w$ is linear, and as the C_w the increase of C_0 basically unchanged. Fig. 9(d) shows that in the process of electrical simulation, if the metallic minerals are dispersed, the content of metallic minerals is increased by gradually replacing the non-conductive minerals with metallic minerals. Therefore, when the content of metallic minerals is less than 80%, the conductivity gradually increases. When the metallic minerals content exceeds 80%, it will gradually replace the conductive components in the rock sample, resulting in a decrease in the overall conductivity. But on the whole, the increase of metallic minerals will increase the conductivity of the reservoir. If the metal minerals are distributed in blocks, the effect on the conductivity is not obvious when the content is less than 10%. This is because when the content is too small, the metallic minerals distributed in blocks cannot form a conductive network. As the content continues to increase, the conductivity gradually increases. From Fig. 9(e), the metallic minerals are distributed in blocks, and the content of metallic minerals in the study area is less than 10%, so the conductivity of metallic minerals is not considered in the conductivity model. Fig. 9(f) confirms that the increase of the conductivity of the organic matter itself is not obvious for the increase of the overall conductivity, indicating that the conductivity of the organic matter itself cannot be discussed when establishing the conductivity model in the study area, but the contribution of the pore water to the reservoir conductivity can be considered. In other words, the organic pores and inorganic pores are not distinguished in this study.

4.2.2. *The influence of pore structure on rock conductivity*

In petrophysical analysis, pore systems govern reservoir storage capacity, while throat geometries predominantly control hydrocarbon productivity by regulating fluid flow permeability (Du and Shi, 2024). Therefore, the study of pore throat is of great significance for reservoir evaluation. In this study, we simulate the influence of pore structure on conductivity by establishing different digital cores to simulate pores with different geometric shapes, different connectivity and different pore radius, and further explain the conductivity mechanism of shale in the study area. The different digital core parameters constructed are shown in Table 5.

Table 3
Common clay minerals of Q_v.

Clay minerals	Q_v, mmol/cm^3
Montmorillonite	5.35
Illite	1.74
Chlorite	0.45

The results of the electrical simulation are shown in Fig. 10. From Fig. 10(a), we can see that with the increase of pore fractal dimension, the more complex and irregular the pore distribution is, the higher the rock conductivity is. When the fractal dimension reaches 2.94, the conductivity increases significantly, and the fractal network forms a multi-level connected path to promote the conductivity of the bulk fluid. As illustrated in Fig. 10(b), under constant clay content, fixed mineral distribution, and invariant porosity, the electrical conductivity of the rock exhibits a notable increase with decreasing coordination number. Conventionally, a higher coordination number is associated with enhanced pore connectivity, which would theoretically improve conductivity. However, this counterintuitive trend can be attributed to the interplay between pore geometry and surface conductivity mechanisms. Specifically, a reduced coordination number implies fewer pore-throat connections but larger individual pore sizes. These enlarged pores tend to retain a greater volume of conductive fluid, while their expanded surface area provides more extensive clay mineral coverage, and the amplified clay-water interface facilitates dominant surface conduction pathways. Under the same porosity, when the clay content and spatial distribution are certain, it can be seen from Fig. 10(c) that the smaller the pore size, the better the overall conductivity of the rock, resulting in low resistance. Compared with the influence of mineral composition, the influence of pore conductive path is more significant. The distribution of pore throats with different sizes reflects the path of fluid flow, which can represent the current path to a large extent. Fig. 10(d) confirms that the digital core simulation results have a good correspondence with the tri-pore-throat classification results mentioned in Section 5.1. The rock sample is relatively dense, and the content of large and medium pore throats is small, which has little effect on the overall conductivity. The content of small pore throats has a great influence on the overall conductivity.

5. Tri-pore-throat conductivity modeling and saturation modeling

5.1. *Tri-pore-throat classification*

Through electrical simulation, the influence of pore structure on conductivity is particularly obvious. Therefore, we further improve the accuracy of the model by studying the pore structure. Shale reservoirs exhibit unique geological characteristics and formation processes, leading to a diverse range of pore types and an exceptionally complex microstructure. This complexity makes the classification of shale pore sizes a challenging task. Although the International Union of Pure and Applied Chemistry (IUPAC) has established widely accepted pore size classification standards—micropores (<2 nm), mesopores (2–50 nm), and macropores (>50 nm)—these criteria, commonly used in chemistry and materials science, may not be entirely suitable for direct application to shale pore studies (Zhang et al., 2017).

Fig. 11 shows the intersection of the water saturation and pore throat radius of the sample piezo mercury in the study area. Based

Table 4
Table of digital core parameters.

Serial number	Q_v, mmol/cm^3	Serial number	V_{clay}, %	Serial number	C_{TOC}, S/m	Serial number	C_w, S/m
A1	3.07560	B1	74.2970	C1	0.0001	D1	0.05
A2	2.92398	B2	52.9220	C2	0.0020	D2	0.10
A3	2.77236	B3	38.6730	C3	0.0200	D3	1.00
A4	2.62074	B4	25.7890			D4	5.00
A5	2.46912	B5	10.1740			D5	11.10
A6	2.31750	B6	5.0868			D6	17.86
A7	2.16588					D7	20.00
A8	2.01426					D8	35.00
A9	1.86264						
A10	1.71102						
A11	1.55940						

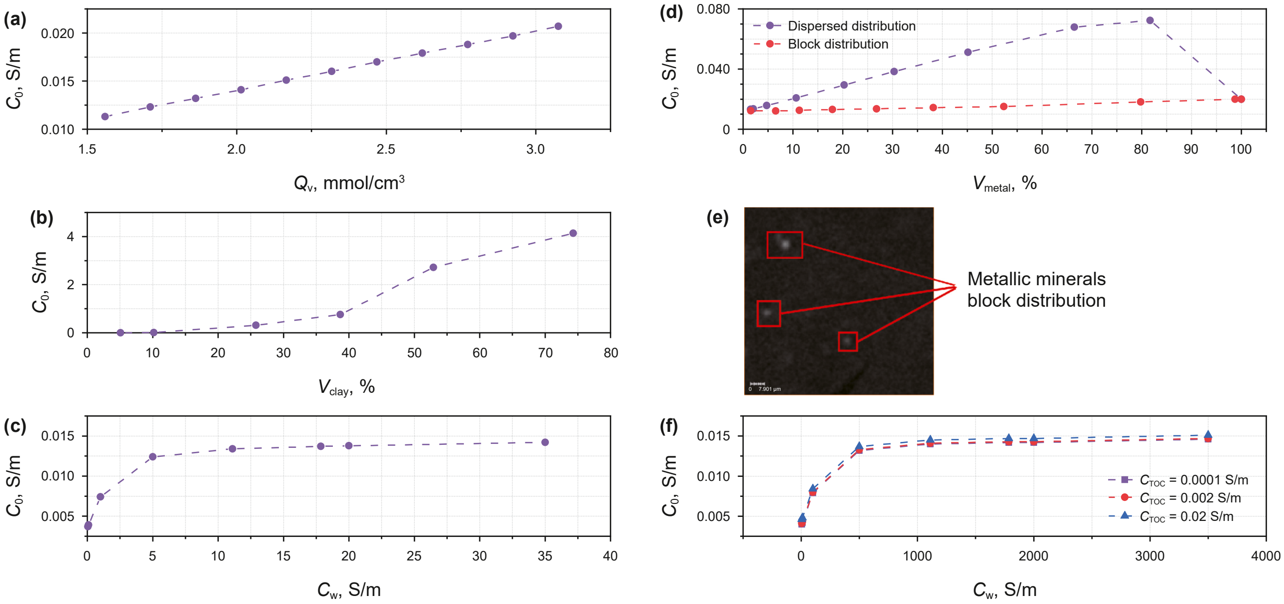

Fig. 9. Conductivity simulation results. **(a)** Digital core simulation results plotted for different cation exchange capacities; **(b)** digital core simulation results plotted for different clay contents; **(c)** digital core simulation results plotted for different formation water mineralization; **(d)** digital core simulation results plotted for different metallic minerals distribution and content; **(e)** the actual distribution form of metallic minerals in the study area; **(f)** digital core simulation results plotted for different C_{TOC}.

Table 5
Table of digital core parameters.

Serial number	Pore fractal dimension	Serial number	Pore coordination number	Serial number	Pore radius (pixel)
E1	2.41	F1	2.57	G1	1
E2	2.57	F2	6.01	G2	2
E3	2.64	F3	15	G3	5
E4	2.84	F4	22.98	G4	10
E5	2.90			G5	20

on the shape of the curve and finding the obvious inflection point of the curve, the following classification scheme is proposed for the shale porosity of the well: the micro-pore-throat (<0.025 μm), the meso-pore-throat (0.025–0.25 μm) and the macro-pore-throat (>0.25 μm).

5.2. Tri-pore-throat model

In the physical model of this paper, the overall resistivity of a rock can be considered as a concatenation of the resistivities formed by three different pore-throat networks. This parallel model reflects the contribution of water in different pore throat segments to the overall electrical conductivity of the rock, where the resistivity of each segment is affected by the conductivity of the water inside it, the pore structure, and the pore connectivity. Its conductive volume model is shown in Fig. 12(a). It is assumed that the metallic minerals in the rock skeleton are electrically conductive, while the other skeleton minerals are not conductive at all. According to the conclusion in Section 4.2, the metallic minerals is also assumed to be non-conductive since the content in all the samples in the study area is too small to form a connected conductive network (You et al., 2023). And assumed that water enters three kinds of pore-throat sizes at the same time and reaches saturation at the same time. Based on these assumptions, a tri-pore-throat saturation model was proposed to be applicable to the quantitative evaluation of low-porosity and low-permeability shale reservoirs.

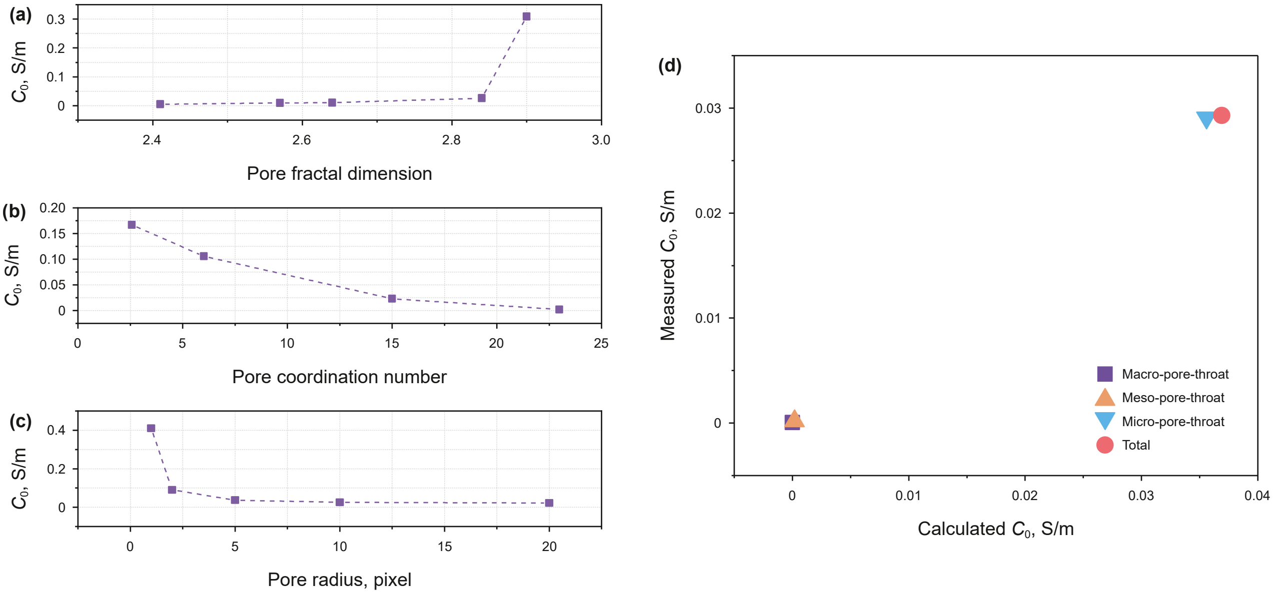

Fig. 10. Conductivity simulation results. **(a)** Digital core simulation results plotted for different pore fractal dimension; **(b)** digital core simulation results plotted for different pore coordination number; **(c)** digital core simulation results plotted for different pore radius; **(d)** cross plot of conductivity digital core simulation for different pore-throat sizes C_0 and tri-pore-throat model calculation C_0.

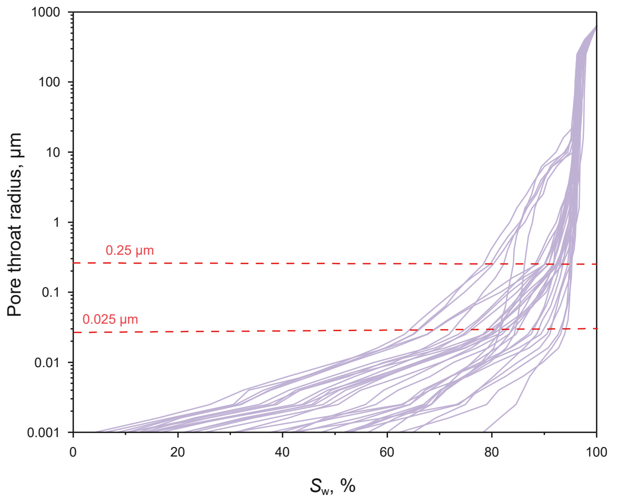

Fig. 11. Intersection of water saturation of rock samples with pore throat radius.

The path of the tri-pore-throat saturation model is formed by the parallel connection of water in three different pore throats. Among them, the pore throat sizes of the different segments are shown schematically in Fig. 12(b).

$$C_0 = C_{\mathrm{ma}} + C_{\mathrm{me}} + C_{\mathrm{mi}} \tag{4}$$

where C_0 denotes the conductivity of 100% water-bearing rock in S/m; C_{ma}, C_{me} and C_{mi} denote the conductivity of the conductive network composed of water in the macro-pore-throat, water in the meso-pore-throat and water in the micro-pore-throat, respectively, when the interior of the formation is saturated with formation water.

The water porosity of the macro-pore-throat, the water porosity of the meso-pore-throat, and the water porosity of the micro-pore-throat can be expressed respectively as ϕ_{ma}, ϕ_{me} and ϕ_{mi}, and the cementation indices corresponding to different pore throats can be expressed as m_{ma}, m_{me} and m_{mi}. The movable water resistivity in the macro-pore-throat and the meso-pore-throat are both the formation water resistivity R_{w}. The electrical conductivity of the water in the micro-pore-throat is different from them, and its resistivity is set to be R_{mc}, so the resistivity response equation for 100% water-bearing rock is:

$$1\Big/R_0 = \phi_{\mathrm{ma}}^{m_{\mathrm{ma}}}\Big/R_{\mathrm{w}} + \phi_{\mathrm{me}}^{m_{\mathrm{me}}}\Big/R_{\mathrm{w}} + \phi_{\mathrm{mi}}^{m_{\mathrm{mi}}}\Big/R_{\mathrm{mc}} \tag{5}$$

where R_0 denotes the resistivity of 100% water-saturated pure rock in units of Ω·m.

Because of the low porosity and low permeability of shale, the water in the micro-pore-throat is bound, so when the reservoir contains hydrocarbons, the movable water in the macro-pore-throat will be replaced by hydrocarbons. Therefore, there is a two-phase seepage process in the macro-pore-throat. Let the percentage of free water in the two-phase fluid be S_{wm}. When the rock contains hydrocarbons, the resistivity and conductivity of the rock are R_{t} and C_{t} respectively, and the resistivity of the rock is related to the degree of saturation, which can be obtained by the Archie formula:

$$1\Big/R_{\mathrm{t}} = \left(S_{\mathrm{wm}}^{n_{\mathrm{m}}}\phi_{\mathrm{ma}}^{m_{\mathrm{ma}}}\right)\Big/R_{\mathrm{w}} + \phi_{\mathrm{me}}^{m_{\mathrm{me}}}\Big/R_{\mathrm{w}} + \phi_{\mathrm{mi}}^{m_{\mathrm{mi}}}\Big/R_{\mathrm{mc}} \tag{6}$$

where n_{m} is the corresponding saturation index; R_{t} is the resistivity of the rock in Ω·m ; S_{wm} is the water saturation of the free pore space in the macro-pore-throat; it can be seen through Eqs. (5) and (6) that in this tri-pore-throat conductivity model, all lithological coefficients are assumed to be equal to 1, and this simplified treatment deviates from the actual situation.

Therefore, on the basis of considering the parallel conductivity of water, the coefficient a related to lithology is introduced, at which time the resistivity response equation of 100% water-bearing rock becomes:

$$1\Big/R_0 = \phi_{\mathrm{ma}}^{m_{\mathrm{ma}}}\Big/(a_{\mathrm{ma}}R_{\mathrm{w}}) + \phi_{\mathrm{me}}^{m_{\mathrm{me}}}\Big/(a_{\mathrm{me}}R_{\mathrm{w}}) + \phi_{\mathrm{mi}}^{m_{\mathrm{mi}}}\Big/(a_{\mathrm{mi}}R_{\mathrm{mc}}) \tag{7}$$

where a_{ma}, a_{me} and a_{mi} are the lithologic coefficients corresponding to the conductive network of water in the macro-pore-

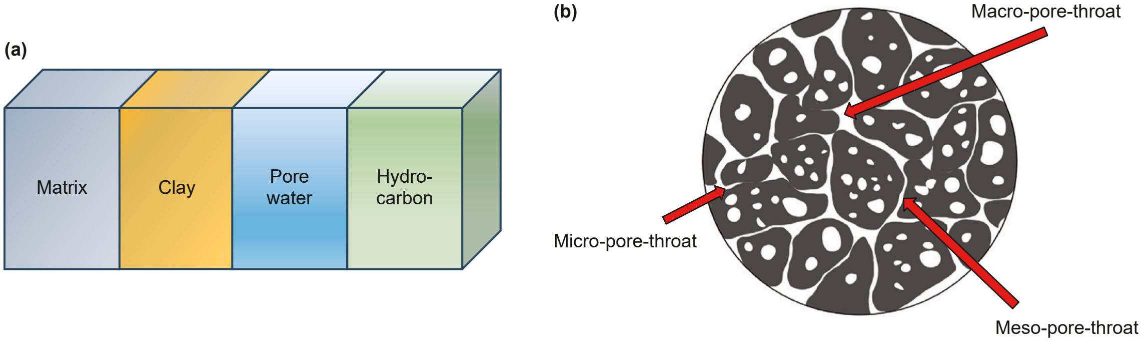

Fig. 12. (**a**) Schematic of the conducting volume model; (**b**) schematic of the tri-pore-throat sizes.

throat, water in the meso-pore-throat, and water in the micro-pore-throat, respectively. These coefficients and parameters were statistically determined by different pore throat sizes.

According to the same considerations as in Eq. (6), it can be obtained by means of the Archie formula:

$$C_t = 1\Big/R_t = \left(S_{wm}^{n_m}\phi_{ma}^{m_{ma}}\right)\Big/(a_{ma}R_w) + \phi_{me}^{m_{me}}\Big/(a_{me}R_w) + \phi_{mi}^{m_{mi}}\Big/(a_{mi}R_{mc}). \tag{8}$$

Comparing Eqs. (6) and (8), it can be found that the improved tri-pore-throat saturation model introduces the lithology parameter a on the basis of the original tri-pore-throat saturation model, which reflects the difference in electrical conductivity of water in different pore throat sections. When the water in the meso-pore and the micro-pore-throats does not exist, the above equation becomes Archie formula, thus highlighting the rationality of the tri-pore-throat saturation model.

We have difficulty in determining the saturation index according to Eq. (8) n_m, and it does not match the measured data from the rock power experiment, so the water saturation equation is modified to:

$$I = b/S_w^n = C_0/C_t \tag{9}$$

$$S_w = \sqrt[n]{C_t/C_0} \tag{10}$$

where n is the saturation index and b is the saturation coefficient. Eqs. (7) and (10) represent the tri-pore-throat conductivity model and the saturation model, respectively, and are collectively referred to as the tri-pore-throat model.

For the sake of narrative convenience, the following is a reference to the usual convention of calling a, b, m, n the rock electric parameters, except for the saturation index n, m_{ma}, a_{ma} are defined as the water petroelectric parameters of the macro-pore-throat; m_{me} and a_{me} are defined as the water-rock electric parameters of the meso-pore-throat; m_{mi} and a_{mi} is defined as the hydraulic-rock electric parameter of the micro-pore-throat.

The parameters related to the water in the tri-pore-throat in the conductivity model need to be given in combination with rock power experiments and experience. The inaccuracy of the parameters will reduce the accuracy of the model to a great extent and seriously limit the effectiveness of the model in practical applications. For this reason, the method of determining the parameters of the tri-pore-throat model needs to be investigated.

1) Determination of the macro-pore-throat ϕ_{ma}:

$$\phi_{ma} = S_{Hg1}\phi_t \tag{11}$$

2) Determination of the meso-pore-throat ϕ_{me}:

$$\phi_{me} = (S_{Hg2} - S_{Hg1})\phi_t \tag{12}$$

3) Determination of the micro-pore-throat ϕ_{mi}:

$$\phi_{mi} = (S_{Hg3} - S_{Hg2})\phi_t \tag{13}$$

where S_{Hg1} is the water saturation of the macro-pore-throat in the mercury compression experiment; S_{Hg2} is the sum of the water saturation of the macro-pore-throat and the meso-pore-throats; S_{Hg3} is the sum of the water saturation of the three pore throats of the rock sample; thus $S_{Hg2} - S_{Hg1}$ is the water saturation corresponding to the meso-pore-throat; $S_{Hg3} - S_{Hg2}$ is the water saturation corresponding to the micro-pore-throat; ϕ_t is the total porosity.

According to the proposed method, we calculated the N rocks in the study area. Substituting the data from N rock samples into Eq. (7), the following system of equations is obtained:

$$1\Big/R_{0j} = \phi_{maj}^{m_{ma}}\Big/(a_{ma}R_w) + \phi_{mej}^{m_{me}}\Big/(a_{me}R_w) + \phi_{mij}^{m_{mi}}\Big/(a_{mi}R_{mc}) \tag{14}$$

where $j \in (0, N)$, $R_{01} - R_{0N}$ is the resistivity of the rock sample calculated by the tri-pore-throat model.

The conductivity obtained by calculated is compared with the measured for verification, as shown in Fig. 13, and the two are in

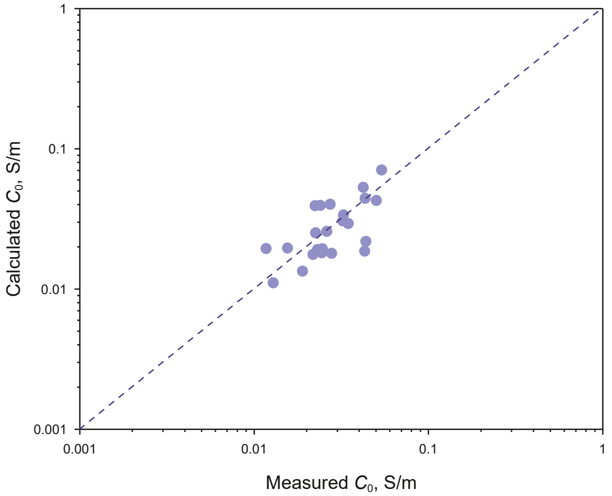

Fig. 13. Comparison between calculated and measured conductivity for the three-hole section model.

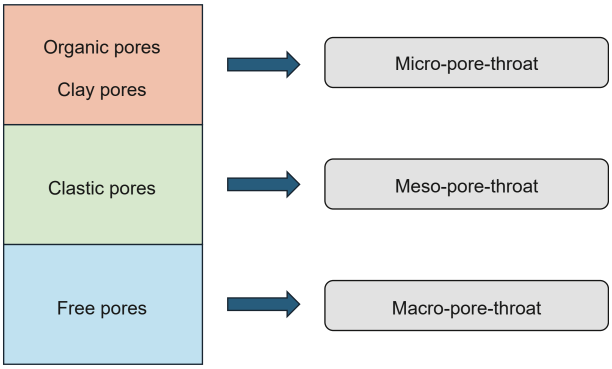

Fig. 14. Schematic diagram of pore types based on pore-throat size.

good conformity, which indicates that the method has a good application effect.

6. Applications in wells

The pore-throat size distribution of shale's organic pores often aligns closely with that of clay pores, as both types are predominantly composed of nano-scale pore-throat sizes. As shown in Fig. 14, given this similarity, these pore types are often considered together in shale reservoir studies (Zhu et al., 2022; Feng et al., 2021).

On the logging scale, nuclear magnetic logging can be directly applied to obtain the pore-throat size distribution curve. In future research, through multi-attribute analysis and artificial intelligence methods, we can also achieve the inversion of reservoir pore throat size (Hosseinzadeh et al., 2024). However, due to the lack of nuclear magnetic logging data in this paper, the following methods are adopted for the application of the new model in the well. It is assumed that both clay minerals and organic matter minerals are micro-pore-throat, and the porosity of micro-pore-throat is calculated by using their content. When containing hydrocarbons, the water in the micro-pore-throat and meso-pore-throat cannot flow from its seepage, so the hydrocarbon replaces the free water. The irreducible water saturation is obtained by mercury injection experiment. The product of irreducible water saturation and total porosity is regarded as the porosity of micro-pore-throat and meso-pore-throat. The difference between irreducible water saturation and total porosity can be used to obtain the macro-pore-throat porosity.

Based on the results of lithological mineral classification, the oil saturation is calculated, the result is shown in Fig. 15. The red rod data is analyzed by closed coring, and the blue part is the data calculated by our model. By subtracting the average of the

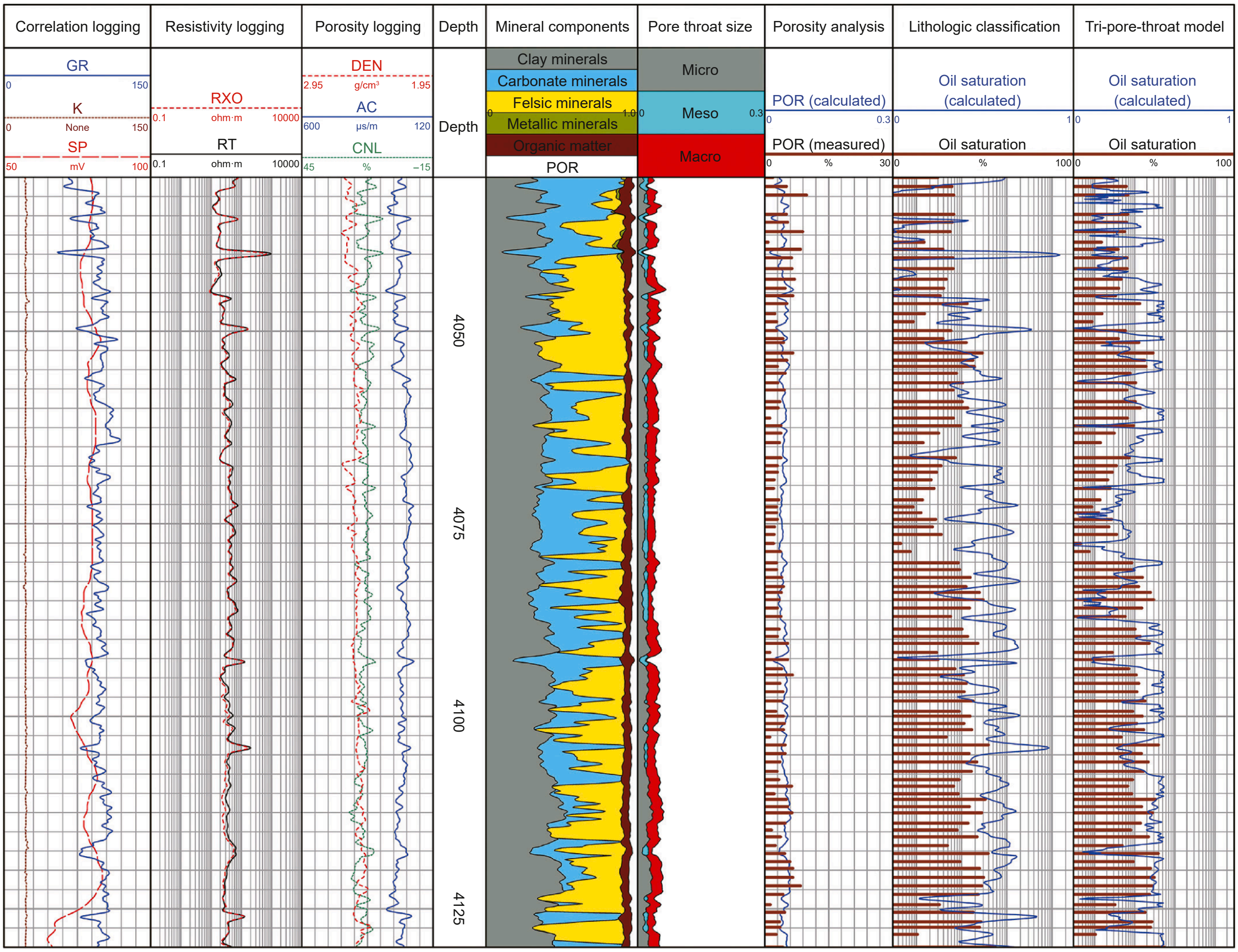

Fig. 15. Comparison of the results of two saturation calculation methods.

measured value and the calculated value, we can get the average absolute error. The average absolute error is 10.983%; the results based on the saturation model of tri-pore-throat system are also shown in Fig. 15, the red rod data is analyzed by closed coring, and the blue part is the data calculated by our model. The average absolute error is 6.481%, and the calculation result is better than that of lithological classification. However, the errors of both classification methods are small, and they have achieved better practical application in the study area.

7. Conclusions

This study investigates the electrical conduction mechanisms of continental shale with complex lithology through mutual validation of experimental petrophysics and computational petrophysics, establishing a theoretical foundation for saturation evaluation in continental shale systems. Our experimental petrophysical analyses reveal that the conventional Archie's equation fails to accurately assess oil saturation in continental shale. Building upon previous research, we propose modifications to adapt Archie's equation for this specific geological context. Recognizing that rock conductivity critically influences Archie parameters, we developed a tailored petrophysical model for the study area by clarifying the underlying conduction mechanisms.

For continental shales with complex mineral compositions, mineral constituents emerge as the dominant factor controlling electrical conductivity. Consequently, we classified the shales based on mineralogical differences and established mineralogy-based saturation models. Results demonstrate enhanced accuracy, with similar m-values across three shale types (indicating analogous pore structure complexity and current pathway tortuosity), while significant n-value variations reflect distinct oil distribution patterns within pores.

Through computational petrophysical modeling, we systematically explored conduction mechanisms: (1) Clay mineral effects: When clay content <40% (typical in this basin), its intrinsic conductivity becomes negligible. (2) Metallic mineral impacts: Metal minerals <10% with blocky distribution fails to form continuous conductive networks, contributing minimally to bulk conductivity.

Given the limited influence of matrix minerals, we designed numerical simulations probing pore structure effects. The influence of the complexity of the pore network and the conductive path of the fluid on the overall electrical conductivity of the rock is more significant than the mineral composition itself. The multi-size pore throat size distribution can reflect the flow space of the fluid, and then reflect the current path. Accordingly, we proposed a tri-pore-throat saturation model based on different pore-throat size characterization. The model is applied to logging, and good results are obtained.

However, this study lacks micro-mechanism research experiments, leaving the conductive behavior of shale organic matter unclear. To address this gap, future research should integrate multi-scale experimental verification. And the lack of nuclear magnetic logging data in logging leads to the problem of pore throat size characterization when applied in logging. Finally, try to apply this saturation evaluation method considering pore throat size to other lithologic reservoirs, such as sandstone, which may verify the wide applicability of the model. In the future, more accurate models will be provided according to artificial intelligence methods.

CRediT authorship contribution statement

Yu-Hang Guo: Writing – original draft, Methodology, Conceptualization, Writing – review & editing, Software, Investigation. **Wan-Ying Wang:** Validation, Project administration, Data curation, Supervision, Methodology. **Bao-Zhi Pan:** Writing – review & editing, Formal analysis, Project administration, Conceptualization. **Shuai Liu:** Project administration, Formal analysis. **Jin-Song Gong:** Methodology. **Li-Hua Zhang:** Writing – review & editing. **Jia-Yi Zuo:** Resources. **Yun-Xiang Gao:** Software. **Xin-Ru Wang:** Software. **Rui-Yi Han:** Validation.

Data availability

The data that has been used is confidential.

Declaration of competing interest

The authors declare that they have no known competing financial interests or personal relationships that could have appeared to influence the work reported in this paper.

Acknowledgements

The work described in this paper is supported by the National Natural Science Foundation of China under Grant 42204122.

References

Alger, R.P., Raymer, L.L., 1963. Formation density log applications in liquid-filled holes. J. Petrol. Technol. 15, 321–332. https://doi.org/10.2118/435-PA.

Amiri, M., Zahedi, G., Yunan, M.H., 2015. Reducing predictive uncertainty in log-derived water saturation models in a giant tight shaly sandstones – A case study from Mesaverde tight gas reservoir. J. Nat. Gas Sci. Eng. 23, 380–386. https://doi.org/10.1016/j.jngse.2015.01.040A.

Andhumoudine, A.B., Nie, X., Zhou, Q., Yu, J., Kane, O.I., Jin, L., Djaroun, R.R., 2021. Investigation of coal elastic properties based on digital core technology and finite element method. Adv. Geo-Energy Res. 5, 53–63. https://doi.org/10.46690/ager.2021.01.06.

Archie, G.E., 1942. The electrical resistivity log as an aid in determining some reservoir characteristics. Trans. AIME 146, 54–62. https://doi.org/10.2118/942054-G.

Chen, T.Y., Hao, Y.Y., Elsworth, D., Zhang, H.M., Hu, Z.M., Cui, G.L., 2023. Modes of multi-mechanistic gas diffusion in shale matrix at varied effective stresses: observations and analysis. Pet. Sci. 20, 2908–2920. https://doi.org/10.1016/j.petsci.2023.03.016.

Clavier, C., Coates, G., Dumanoir, J., 1984. Theoretical and experimental bases for the dual-water model for interpretation of shaly sands. Soc. Petrol. Eng. J. 24, 153–168. https://doi.org/10.2118/6859-PA.

De Witte, L., 1955. A study of electric log interpretation methods in shaly formations. Trans. AIME 204, 103–110. https://doi.org/10.2118/402-G.

Du, S.H., Shi, Y.M., 2024. Concise extraction and characterization of the pore-throat network in unconventional hydrocarbon reservoirs: A new perspective. Pet. Sci. 21 (3), 1474–1487. https://doi.org/10.1016/j.petsci.2023.12.009.

Fan, Y., Pan, B., Mo, X., Guo, Y., Lei, J., 2020. Study on the C_0–C_w relationship of clay-bearing sandstones based on digital cores. Acta Geophys. 68, 641–649. https://doi.org/10.1007/s11600-020-00410-7.

Feng, C., Feng, J., Feng, Z., Zhong, Y., Mao, Z., Ling, K., 2021. Determination of reservoir wettability based on resistivity index prediction from core and log data. J. Petrol. Sci. Eng. 205, 108842. https://doi.org/10.1016/j.petrol.2021.108842.

Fu, Q., Hu, Z., Feng, D., Huang, J., Xing, L., Zhu, Z., Teng, W., 2023. Restoration and evolution of the Paleogene (E_1f_2) shale sedimentary environment in the Subei Basin, China. ACS Omega 8, 46892–46903. https://doi.org/10.1021/acsomega.3c06603.

Gao, H., Qing, L., Ma, G., Zhang, D., Wei, C., 2024. Numerical investigation into effects of rheological properties on grout flow in rock fracture using Herschel-Bulkley model. Eng. Geol. 329, 107402. https://doi.org/10.1016/j.enggeo.2023.107402.

Givens, W.W., 1987. A conductive rock matrix model (CRMM) for the analysis of low-contrast resistivity formations. Log. Anal. 28.

Gupta, A.R., Kamal, 2023. A theoretical approach for water saturation estimation in shaly sandstones. Geoenergy Sci. Eng. 228, 212001. https://doi.org/10.1016/j.geoen.2023.212001.

Hasan, M.F., Abuel-Naga, H., Leong, E.C., 2021. A modified series-parallel electrical resistivity model of saturated sand/clay mixture. Eng. Geol. 290, 106193. https://doi.org/10.1016/j.enggeo.2021.106193.

Hosseinzadeh, S., Mollajan, A., Akbarzadeh, S., Kadkhodaie, A., 2024. Rock type based-estimation of pore throat size distribution in carbonate reservoirs using integrated analysis of well logs and seismic attributes. Carbonates Evaporites 39, 46. https://doi.org/10.1007/s13146-024-00954-5.

Hu, X., Cheng, R., Zhang, H., Zhu, J., Chi, P., Sun, J., 2024. Three-water differential parallel conductivity saturation model of low-permeability tight oil and gas reservoirs. Energies 17, 1726. https://doi.org/10.3390/en17071726.

Kadkhodaie, A., Rezaee, R., 2016. A new correlation for water saturation calculation in gas shale reservoirs based on compensation of kerogen-clay conductivity. J. Petrol. Sci. Eng. 146, 932–939. https://doi.org/10.1016/j.petrol.2016.08.004.

Lai, F., Liu, Y., Tan, X., Wang, R., Peng, S., Gao, X., 2024. A composite water saturation model of continental mixed shale oil reservoirs based on complex lithology identification. Geol. J. 59, 1401–1415. https://doi.org/10.1002/gj.4934.

Li, B., Nie, X., Cai, J., Zhou, X., Wang, C., Han, D., 2022. U-Net model for multi-component digital rock modeling of shales based on CT and QEMSCAN images. J. Petrol. Sci. Eng. 216, 110734. https://doi.org/10.1016/j.petrol.2022.110734.

Li, X., Li, B., Liu, F., Li, T., Nie, X., 2023. Advances in the application of deep learning methods to digital rock technology. Adv. Geo-Energy Res. 8, 5–18. https://doi.org/10.46690/ager.2023.04.02.

Liu, X., Sun, J., Wang, H., 2009. Numerical simulation of rock electrical properties based on digital cores. Appl. Geophys. 6, 1–7. https://doi.org/10.1007/s11770-009-0001-6.

Liu, X., Lai, J., Fan, X., Shu, H., Wang, G., Ma, X., Liu, M., Guan, M., Luo, Y., 2020. Insights in the pore structure, fluid mobility and oiliness in oil shales of Paleogene Funing Formation in Subei Basin, China. Mar. Petrol. Geol. 114, 104228. https://doi.org/10.1016/j.marpetgeo.2020.104228.

Mashaba, V., Altermann, W., 2015. Calculation of water saturation in low resistivity gas reservoirs and pay-zones of the Cretaceous Grudja Formation, onshore Mozambique basin. Mar. Petrol. Geol. 67, 249–261. https://doi.org/10.1016/j.marpetgeo.2015.05.016.

Moradi, M., Kadkhodaie, A., 2024. The impact of geological and petrophysical heterogeneities on Archie's exponents: A case study for Sarvak carbonate reservoir, Dezful Embayment, southwest Iran. Carbonates Evaporites 39, 1–19. https://doi.org/10.1007/s13146-024-00945-6.

Nie, X., Zou, C., Li, Z., Meng, X., Qi, X., 2016. Numerical simulation of the electrical properties of shale gas reservoir rock based on digital core. J. Geophys. Eng. 13, 481–490. https://doi.org/10.1088/1742-2132/13/4/481.

Norbisrath, J.H., Eberli, G.P., Laurich, B., Desbois, G., Weger, R.J., Urai, J.L., 2015. Electrical and fluid flow properties of carbonate microporosity types from multiscale digital image analysis and mercury injection. Bulletin 99, 2077–2098. https://doi.org/10.1306/07061514205.

Poupon, A., Loy, M.E., Tixier, M.P., 1954. A contribution to electrical log interpretation in shaly sands. J. Petrol. Technol. 6, 27–34. https://doi.org/10.2118/311-G.

Qin, Z., Wu, D., Luo, S., Ma, X., Huang, K., Tian, F., Xiao, K., Chen, X., Hou, M., Pan, H., 2020. A novel method to obtain permeability in a dual-pore system using geophysical logs: a case study of an Upper Triassic Formation, Southwest Ordos Basin, China. Nat. Resour. Res. 29, 2619–2634. https://doi.org/10.1007/s11053-019-09612-3.

Qin, Z., Wang, G., Zhang, Y., Wang, C., Wu, J., Su, K., Wei, K., Deng, C., Ma, C., Xiao, K., Pan, H., Hu, X., 2023. A novel evaluation scheme of resistivity anisotropy in near-tight sandstones using conventional geophysical logs: A case study of the Triassic Chang 8 oil layer, Zhenjing area, Ordos Basin. J. Appl. Geophys. 213, 105017. https://doi.org/10.1016/j.jappgeo.2023.105017.

Sam-Marcus, J., Enaworu, E., Rotimi, O.J., Seteyeobot, I., 2018. A proposed solution to the determination of water saturation: using a modelled equation. J. Pet. Explor. Prod. Technol. 8, 1009–1015. https://doi.org/10.1007/s13202-018-0453-4.

Schlumberger, 1989. Log Interpretation Principles/Applications. Seventh Printing. Schlumberger Well Service Inc., Sugar Land, pp. 8–14.

Simandoux, P., 1963. Mesures Dielectriques En Milieu Poreux, Application a Mesure Des Saturations En Eau, Etude Du Comportment Des Massifs Argileux. Revue de l'Institut Français du Pétrole, n Hors-Série, pp. 193–215 (in French).

Sun, J., Feng, P., Chi, P., Yan, W., 2022. Microscopic conductivity mechanism and saturation evaluation of tight sandstone reservoirs: A case study from Bonan Oilfield, China. Energies 15, 1368. https://doi.org/10.3390/en15041368.

Tian, J., Wang, L., Ostadhassan, M., Zhang, L., Liu, H., Sima, L., 2024. Pore structure exponent of Archie's law in a dual-porosity medium: vuggy reservoirs. Geoenergy Sci. Eng. 234, 212659. https://doi.org/10.1016/j.geoen.2024.212659.

Wang, Y., Li, X., Chen, B., Wu, W., Dong, D., Zhang, J., Han, J., Ma, J., Dai, B., Wang, H., Jiang, S., 2018. Lower limit of thermal maturity for the carbonization of organic matter in marine shale and its exploration risk. Petrol. Explor. Dev. 45, 402–411. https://doi.org/10.1016/S1876-3804(18)30045-4.

Wang, Z., Li, H., Lan, X., Wang, K., Yang, Y., Lisitsa, V., 2021. Formation damage mechanism of a sandstone reservoir based on micro-computed tomography. Adv. Geo-Energy Res. 5, 25–38. https://doi.org/10.46690/ager.2021.01.04.

Wang, S., Tan, M., Wang, X., Zhang, L., 2022. Microscopic response mechanism of electrical properties and saturation model establishment in fractured carbonate rocks. J. Petrol. Sci. Eng. 208, 109429. https://doi.org/10.1016/j.petrol.2021.109429.

Wang, J., Guo, Q., Chen, X., Liu, Z., Bai, X., Fan, L., He, W., 2024. Geological characteristics and resource potential of shale oil in major basins of China. Petrol. Sci. Technol. 42, 1533–1565. https://doi.org/10.1080/10916466.2022.2147544.

Waxman, M.H., Smits, L.J.M., 1968. Electrical conductivities in oil-bearing shaly sands. Soc. Petrol. Eng. J. 8, 107–122. https://doi.org/10.2118/1863-A.

Wei, W., Cai, J., Hu, X., Han, Q., 2015. An electrical conductivity model for fractal porous media. Geophys. Res. Lett. 42, 4833–4840. https://doi.org/10.1002/2015GL064460.

Wu, F., Wen, Z., Yao, C., Wang, X., Xi, Y., Cong, L., 2020. Numerical simulation of the influence of pore structure on resistivity, formation factor and cementation index in tight sandstone. Acta Geologica Sinica – English Edition 94, 290–304. https://doi.org/10.1111/1755-6724.14306.

Xu, J., Xu, L., Qin, Y., 2017. Two effective methods for calculating water saturations in shale-gas reservoirs. Geophysics 82, D187–D197. https://doi.org/10.1190/geo2016-0462.1.

You, F., Liu, G., Sun, M., An, C., Li, C., Li, Y., 2023. Impacts of pore structure on the occurrence of free oil in lacustrine shale pore networks. Energies 16, 7205. https://doi.org/10.3390/en16207205.

Zha, X., Lai, F., Gao, X., Gao, Y., Jiang, N., Luo, L., Li, Y., Wang, J., Peng, S., Luo, X., Tan, X., 2021. Characteristics and genetic mechanism of pore throat structure of shale oil reservoir in saline lake—A case study of shale oil of the Lucaogou Formation in Jimsar Sag, Junggar Basin. Energies 14, 8450. https://doi.org/10.3390/en14248450.

Zhang, P., Lu, S., Li, J., Xue, H., Li, W., 2017. Characterization of shale pore system: a case study of Paleogene Xin'gouzui Formation in the Jianghan Basin, China. Mar. Petrol. Geol. 79, 321–334. https://doi.org/10.1016/j.marpetgeo.2016.10.014.

Zhao, J., Sun, J., Liu, X., Chen, H., Cui, L., 2013. Numerical simulation of the electrical properties of fractured rock based on digital rock technology. J. Geophys. Eng. 10, 055009. https://doi.org/10.1088/1742-2132/10/5/055009.

Zhou, Y., Zhong, X., Nie, X., 2024. Identification and parameter characterization of pores and fractures in shales based on multi-scale digital core data. Adv. Geo-Energy Res. 13, 146–160. https://doi.org/10.46690/ager.2024.08.08.

Zhu, L., Ma, Y., Cai, J., Zhang, C., Wu, S., Zhou, X., 2022. Key factors of marine shale conductivity in southern China—Part II: the influence of pore system and the development direction of shale gas saturation models. J. Petrol. Sci. Eng. 209, 109516. https://doi.org/10.1016/j.petrol.2021.109516.